ELSEVIER

Journal of Nuclear Materials 317 (2003) 54–61

journal of nuclear materials

www.elsevier.com/locate/jnucmat

Thermal expansion characteristics of a titanium modified austenitic stainless steel: measurement by high-temperature X-ray diffraction and modelling using Grüneisen formalism

R. Jose [a], S. Raju [a,*], R. Divakar [a], E. Mohandas [a], G. Panneerselvam [b], M.P. Antony [b], K. Sivasubramanian [c]

[a] *Physical Metallurgy Section, Materials Characterisation Group, Indira Gandhi Centre for Atomic Research, Kalpakkam 603 102, India*
[b] *Fuel Chemistry Division, Indira Gandhi Centre for Atomic Research, Kalpakkam 603 102, India*
[c] *Safety Engineering Division, Indira Gandhi Centre for Atomic Research, Kalpakkam 603 102, India*

Received 19 August 2002; accepted 5 December 2002

Abstract

The thermal expansion of a titanium modified, swelling resistant austenitic stainless steel designated as D9 is studied by measuring the lattice parameter as a function of temperature in the range 300–1300 K by high-temperature X-ray diffraction technique. The thermal expansion data thus obtained is in reasonable agreement with the typical thermal expansion values reported for similar nuclear grade austenitic stainless steels. However, at temperatures exceeding 900 K, the measured thermal expansivity exhibits a pronounced non-linear increase due partly to the precipitation of complex carbide and intermetallic phases. The high-temperature thermal expansion data obtained in the present study are augmented by modelling the low-temperature thermal expansion behaviour by Grüneisen formalism.

PACS: 65.70; 61.10

1. Introduction

It is well known that accurate information on various thermophysical properties of materials is essential for a knowledge-based design of engineering components. This requirement becomes even more crucial, if the material under consideration is expected to perform in a demanding ambience. In fact, such is the case of various structural materials that go into the construction of a nuclear reactor. The material under present study, namely a titanium modified, controlled carbon content austenitic stainless steel is currently a probable candidate material for the fuel clad and wrapper tubes of India's first 500-MWe prototype fast breeder reactor (PFBR) [1]. This stainless steel is designated as D9. The design philosophy of this steel is based on the objective of achieving an enhanced swelling resistance, in combination with optimal mechanical and chemical properties. A typical composition of this steel (melted at MIDHANI, India) as determined through optical emission spectroscopy is listed in Table 1, together with that of AISI-304, 304L, 316, 316LN, 321 and the American version of D9 studied by Leibowitz and Blomquist [2] for comparative purposes. As can be seen, the nominal composition of this stainless steel is designed to be around that of AISI-316, but with the important exception of having high-nickel (correspondingly low-chromium), besides controlled titanium additions. The comparatively high-nickel composition is aimed at achieving a larger incubation time for the onset of steady-state swelling [3]. The titanium to carbon ratio

* Corresponding author. Tel.: +91-4114 480306; fax: +91-4114 480081.
E-mail address: sraju@igcar.ernet.in (S. Raju).

0022-3115/03/$ - see front matter
doi:10.1016/S0022-3115(02)01701-4

Table 1
Nominal chemical composition in weight percent of the titanium modified stainless steel (D9) investigated in the present study together with that for some typical austenitic stainless steels of AISI-300 series

Element	304[a]	304L[b]	316[a]	316LN[c]	321[d]	D9[e]	D9[f]
Ni	9.7	9.3	11.7	12.5	9.0–12.0	14.7 ± 3.0	15.5
Cr	18.4	18.5	16.8	18.0	17.0–19.0	15.0 ± 0.4	13.5
Mn	1.4	1.16	1.9	1.6–2.0	<2.00	1.5 ± 0.5	2.0
Mo		0.15	2.1	2.7		2.2 ± 0.1	2.0
Cu		0.1	0.2	1.0		<0.050	
Ti					$\geqslant 5\times$%C	0.3 ± 0.002	0.25
Nb						<0.167	
V						0.06 ± 0.002	
Co		0.18		0.25		0.04 ± 0.002	
Al						<0.034	
Sn						<0.004	
W						0.005	
Si	0.6	0.7	0.4	0.05	$\leqslant 1.00$	0.67 ± 0.03	0.75
C	0.02	0.022	0.05	0.03	$\leqslant 0.08$	0.05 ± 0.004	0.04
N		0.010		0.08			
P	0.02	0.010	0.03	0.035	$\leqslant 0.045$	0.009 ± 0.001	
S	0.01	0.011	0.02	0.025		0.008 ± 0.003	
B				0.002			
As						<0.006	
Fe	Balance	Balance	Balance	Balance	Balance	Balance	
Density at ~300 K ($kg\,m^{-3}$)	~7860	~8000	~7970	~7966		~7997[g]	

It must be stated that in general there is a considerable scatter in the stated compositions of the same steel by different investigators and what is quoted here are those compositions for which reliable experimental data on thermal and elastic properties are available [2,14–20].

[a] Taken from Ref. [20].

[b] Taken from Refs. [16,19].

[c] Taken from (IGCAR internal report: PFBR/01000/DN/1000).

[d] Taken from Ref. [17].

[e] Determined in this study by direct reading optical emission spectrometer.

[f] Taken from Ref. [2].

[g] Density determined in the present study by immersion technique.

is optimised in conjunction with the extent of cold work (roughly about 20%) to obtain a small volume fraction (<5%) of very fine dispersion of heterogeneously nucleated TiC precipitates in an otherwise feature free austenitic matrix [4]. Although the details of the atomistic mechanisms through which the very fine TiC precipitate network enhances the swelling resistance are not known at present, it is believed that the matrix/TiC interface would be playing a significant role in accommodating the radiation damage [5]. A precise knowledge of thermal expansion and elastic property of the austenitic matrix is therefore necessary in quantifying the extent of interfacial strain and hence its influence in effectively sinking the irradiation induced defects.

A general survey revealed that there exists in open literature very little information on various thermal and elastic properties of this stainless steel. To the best of our knowledge, apart from the dilatometric study of bulk thermal expansion by Leibowitz and Blomquist [2] on a steel of similar composition (Table 1) and the recent heat capacity data of Nawada et al. [6], we could gather no other specific information regarding thermal and elastic properties from the open literature. Further, an X-ray diffraction study of the thermal expansion of this steel has not been reported so far.

The present study attempts to fill this gap. The lattice thermal expansion of the austenite matrix is monitored by high-temperature X-ray diffractometry (HT-XRD) in the range 300–1300 K. In addition, the high-temperature thermal expansivity data thus generated is augmented by modelling the corresponding low-temperature thermal expansion by a Grüneisen formalism.

2. Experimental procedure

The material for this study is procured from MIDHANI, India in the form of a forged rod of about 1.5 cm diameter, from which a thin slice is precision cut and cold rolled to foils of about 80 μm thickness. These

foils are then solution annealed at 1323 K for about 24 h in an inert atmosphere. A thin rectangular strip of about 2 cm × 0.5 cm cut from the annealed foil is used in HT-XRD studies. An optimal thickness of about 80 μm for the sample is chosen as a compromise between ensuring minimal temperature gradient across its thickness, while reducing at the same time an undue buckling due to thermal stresses. The buckling of the foil results in a mild distortion of the diffraction geometry and hence causes an apparent shift in the measured 2θ values [7]. The high-temperature X-ray diffraction experiment is performed in a Philips-X'pert MPD® system equipped with a high-vacuum (better than 10^{-5} mbar) heating stage consisting of a resistance heated thin flat tantalum foil as the heater. The temperature of the tantalum heater is measured by a Pt–Rh thermocouple, spot-welded to its bottom portion and is controlled to an accuracy of ±1 K. The temperature is gradually raised from room temperature to 1300 K in steps of 100 K at the rate of about 1 K/min. The sample is kept for about 60 min at each temperature in order to ensure thermal equilibrium. α-alumina is used as the standard for 2θ calibration purposes. Owing to the finite thickness of the sample foil, there is a small difference in temperature between that measured by the thermocouple and the one experienced by the actual sample surface. This is corrected by co-recording the diffraction pattern of the tantalum heater foil at identical temperatures and correcting the measured lattice parameter *versus* temperature data of tantalum against the critically assessed thermal expansion data of Reeber and Wang [8].

3. Results

3.1. General

Fig. 1(a) and (b) present respectively the room temperature and high-temperature diffraction patterns recorded in the present study. The 2θ–d_{hkl} listing is provided in Table 2. The lattice parameters were estimated from the three main reflections of the austenitic matrix and an effective high-angle corrected lattice constant is obtained by the Nelson–Riley interpolation procedure [9]. The corrected lattice parameter at each temperature is listed in Table 2. The experiments are repeated twice at each temperature and a good reproducibility has been achieved. The estimated lattice constants are generally accurate to ±0.0001 nm even at high-temperatures, as found by comparing the measured lattice parameters of α-alumina and tantalum with the corresponding reference data [8,10]. The lattice parameter at 300 K for our stainless steel is found to be 0.35903 nm. The measured lattice parameter values in the range 300–1300 K are fitted to the following third order polynomial in temperature increment ($T - 300$).

$$a\ (\mathrm{nm}) = 0.35903 + 4.3546 \times 10^{-6}(T-300) + 7.4165 \times 10^{-10}(T-300)^2 + 1.5321 \times 10^{-12}(T-300)^3. \quad (1)$$

The temperature dependence of the measured lattice parameter is portrayed graphically in Fig. 2. Eq. (1) has been used to calculate the true or instantaneous (α_i), relative (α_r) and mean (α_m) linear thermal expansivities defined by the following relations:

$$\alpha_i = 1/a_T\{\partial a_T/\partial T\}_P, \quad (2)$$

$$\alpha_r = 1/a_0\{\partial a_T/\partial T\}_P, \quad (3)$$

$$\alpha_m = 1/a_0\{(a_T - a_0)/(T - T_0)\}_P. \quad (4)$$

In the above equations, a_0 represents the lattice parameter at 300 K. The volume thermal expansivity can be obtained by multiplying the corresponding linear expansion coefficient by a factor three since we are dealing with a cubic system. The experimental thermal expansion values are compared with the reported thermal expansion data for other similar austenitic stainless steels in Fig. 3.

3.2. Comparison with other thermal expansion data

At the outset, it must be mentioned that there exists no XRD based thermal expansion data for this stainless steel. However, the mean bulk thermal expansion values reported by Leibowitz and Blomquist [2] for a similar steel, but with slightly different composition (Table 1) is somewhat higher than the present data. Further, upon comparing the present thermal expansivity values with the literature data on other related nuclear grade steels, it emerges, that our XRD based thermal expansion data is well within the range that is typical of austenitic stainless steels (Fig. 3).

One other important point regarding the present thermal expansion data is concerned with the gradual non-linear increase noticed from about 900 K. It is well known that such non-linearity can come from a variety of sources like lattice anharmonicity and point defects. However, we believe that in the present case, subtle precipitation effects aided especially by the cumulative high-temperature holds inherent in our experimental schedule also serve to complicate the high-temperature thermal expansion behaviour. It must be stated that during the course of experiments, we noticed the precipitation of some complex carbide and intermetallic phases at temperatures starting from 900 K onwards. The precipitation of such hard complex phases strains the austenitic matrix so much that at high-temperatures it experiences the thermal expansion under stressed conditions. A detailed study of this high-temperature precipitation process is currently underway.

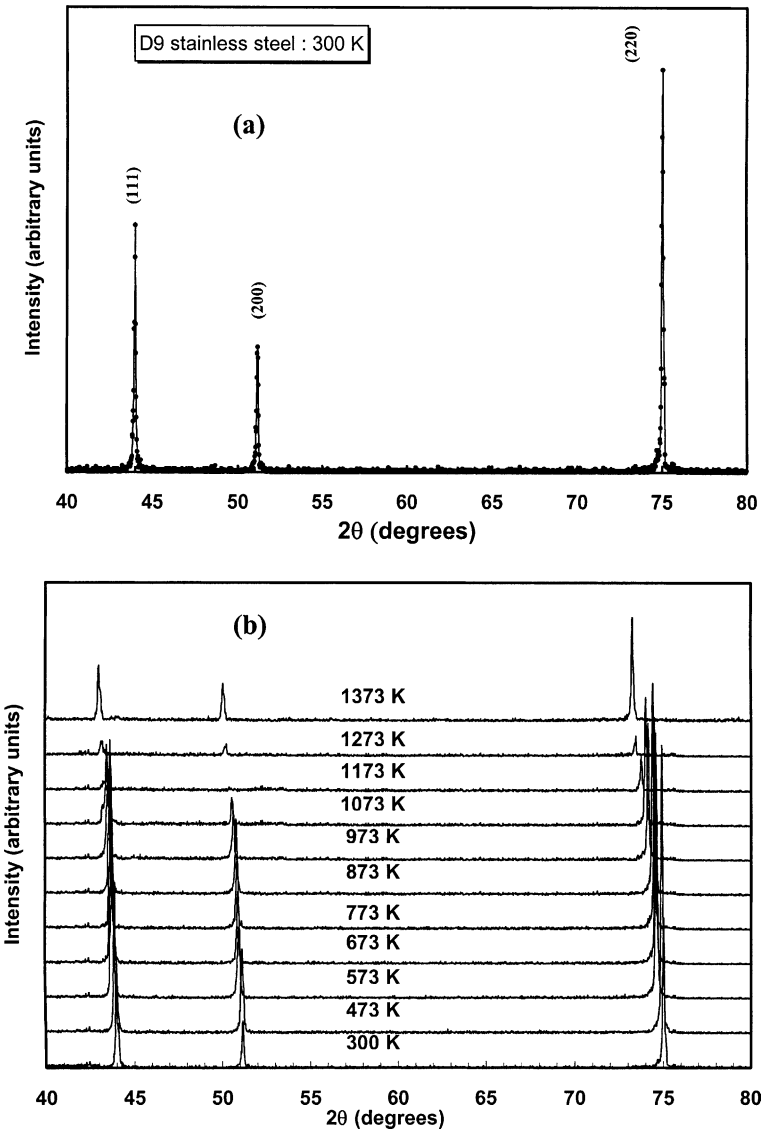

Fig. 1. The X-ray diffraction pattern of D9 sample taken at 300 K (a) and at higher temperatures (b).

As a passing remark, it may also be mentioned that low-temperature thermal expansion measurements are also lacking for this stainless steel. Since the lattice contribution to the low-temperature heat capacities of many austenitic stainless steels can be approximated by a simple Debye model [11], we presume that such a homologous character also holds good for our D9 steel. In view of this, we have attempted to simulate the low-temperature specific heat and thermal expansion by invoking the time-honoured Grüneisen formalism [12,13]. The details of this methodology are outlined by Wachtman et al. [12] and also by Suzuki [13].

3.3. Estimation of low-temperature thermal expansion

In Fig. 4, we present a summary of the available low and high-temperature heat capacity data for some technologically relevant austenitic stainless steels. The required data come from varied sources and experimental methods [14–19]. It is quite evident from Fig. 4, that as for the low-temperature specific heat is concerned; the austenitic stainless steels exhibit a common behaviour. The electronic specific heat coefficient (γ_e) and the Debye temperature (θ_D) estimated from these data are listed in Table 3. By assuming a homologous nature of bonding forces to be prevailing in materials of

Table 2
Listing of X-ray diffraction data at various temperatures

T (K)	2θ experimental (deg)			$\pm 2\theta$ correction factor (deg)	d_{hkl} values (corrected) (nm)			Lattice parameter measured (nm)	Lattice parameter fitted to Eq. (1) (nm)
	(1 1 1)	(2 0 0)	(2 2 0)		(1 1 1)	(2 0 0)	(2 2 0)		
300	43.9699	51.1647	75.0204	0.1004	0.20542	0.17815	0.12642	0.35895	0.35903
473	43.9119	51.1307	74.9227	0.0597	0.20585	0.17839	0.12662	0.35935	0.35972
573	43.7698	50.9337	74.6095	0.0420	0.20657	0.17909	0.12709	0.36081	0.36021
673	43.7473	50.8725	74.5665	0.0285	0.20673	0.17934	0.12718	0.36102	0.36076
773	43.7079	50.8386	74.5031	0.0192	0.20695	0.17948	0.12728	0.36125	0.36138
873	43.6604	50.7865	74.3987	0.0142	0.20719	0.17967	0.12744	0.36174	0.36207
973	43.5354	50.6520	74.1394	0.0134	0.20775	0.18012	0.12783	0.36290	0.36281
1073	43.4717	50.5475	74.0105	0.0168	0.20803	0.18045	0.12801	0.36348	0.36362
1173	43.3700	50.4472	73.7660	0.0244	0.20846	0.18076	0.12836	0.36460	0.36450
1273	43.2697	50.2370	73.5857	0.0363	0.20886	0.18143	0.12862	0.36542	0.36544
1373	43.0045	49.9961	73.2454	0.0524	0.21001	0.18219	0.12910	0.36631	0.36645

The correction factor for 2θ is estimated by comparing the diffraction data of the reference materials, namely α-alumina and tantalum with their recommended lattice parameters [8,10]. Refer to text for details.

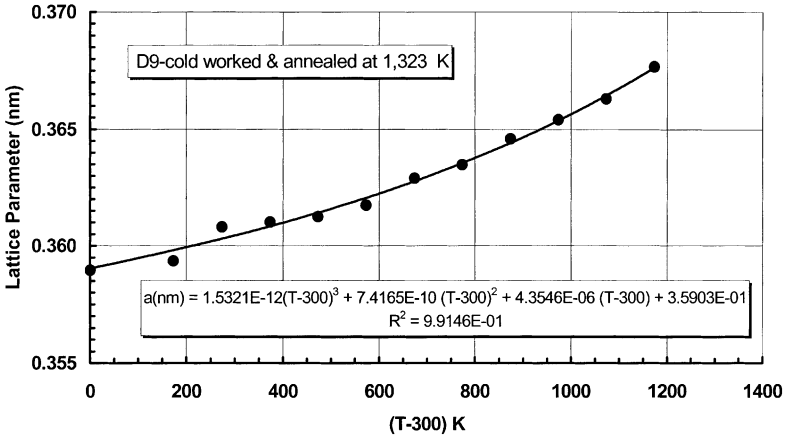

Fig. 2. The variation of the lattice parameter of the austenitic matrix is plotted as a function of temperature. The filled circles represent the experimental points. The line represents the cubic fit obtained by the method of least squares.

similar structural and cohesion class, we use the existing data on Debye temperature and density of 304 and 316 stainless steels to arrive at a first order estimate of the Debye temperature of our D9-steel. For this purpose, we measured the density of our steel by the standard immersion technique. The value of the measured density is 7.997×10^3 kg m^{-3}. The estimated θ_D is found to be 456 K. The average molar weight ($\overline{M}$) of our steel is calculated from the measured bulk density by the following formula.

$$\rho = n\overline{M}/(VN_A). \tag{5}$$

In Eq. (5), ρ stands for density in kg m^{-3}; V represents the volume of the unit cell in m^3; N_A is the Avogadro number; and n is the effective number of atoms per unit cell. Here we take $n = 4.2$ in accordance with the requirement that the measured and the approximately estimated density from the chemical composition should agree on a nominal basis. For our D9 steel, the average molar mass thus estimated turns out to be 56.405.

According to Wachtman et al. [12], the temperature dependence of volume can be written within the spirit of Grüneisen's approximation in the following manner.

$$V_T = V_0\{U/(Q_0 - kU) + 1\}. \tag{6}$$

The corresponding expression for the volume thermal expansivity can be obtained by differentiating Eq. (6) with respect to temperature.

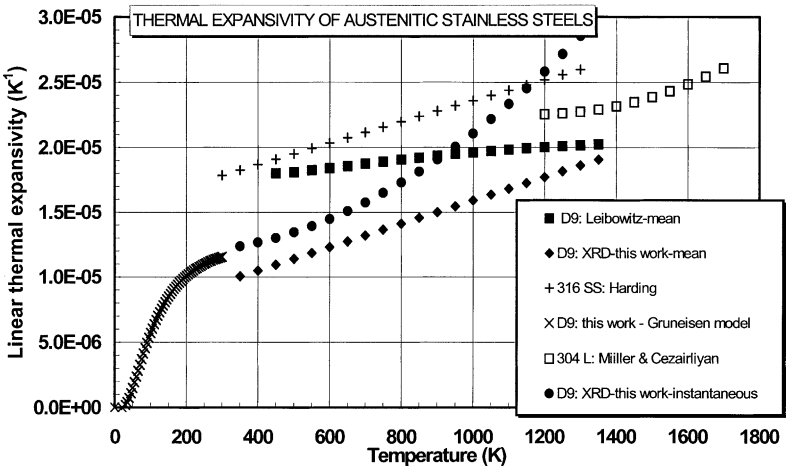

Fig. 3. The temperature dependence of the experimentally obtained high-temperature thermal expansivity is graphically portrayed along with the literature data on other related materials. The crosses in the figure stand for the estimated low-temperature data using Grüneisen formalism.

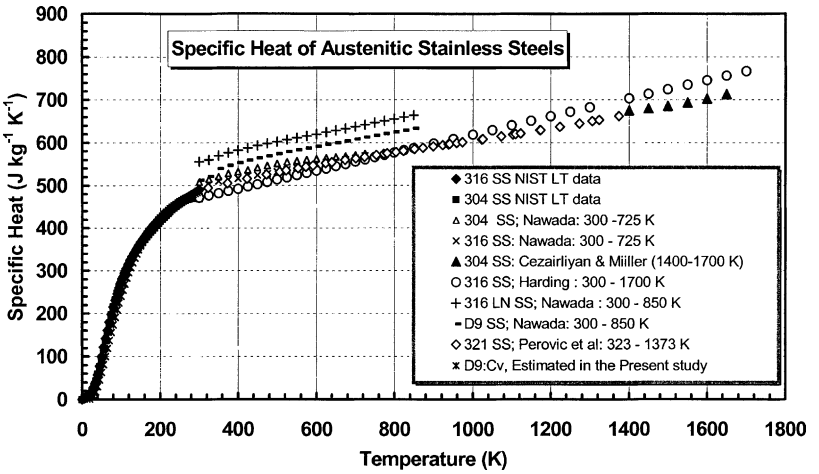

Fig. 4. The available data on low and high-temperature specific heat of some nuclear grade austenitic stainless steels are plotted as a function of temperature. Note that the low-temperature specific heats of various austenitic stainless steels are almost overlapping with each other, thus supporting a possible homologous character of bonding forces in them.

$$\alpha_V = (Q_0 C_V)/\{(k(k-1)U^2) - (Q_0(2k-1)U) + (Q_0^2)\}. \tag{7}$$

$$Q_0 = V_0 B_0/\gamma_G. \tag{8}$$

$$k = (B_0'1)/2. \tag{9}$$

In Eqs. (6)–(9), V_T stands for the specific volume at temperature T, V_0, the corresponding quantity at 300 K, U is the internal energy or more appropriately the vibrational contribution to the internal energy, C_V is the isochoric specific heat, B_0 is the isothermal bulk modulus at 300 K, B_0' is the pressure derivative of B_0 and γ_G is the Grüneisen parameter taken to be temperature independent. The internal energy and the constant-volume specific heat can be estimated in terms of Debye model. Alternately, one can also adopt the equivalent Nernst–Lindemann approximation for U and C_V [12]. The relevant expressions for U and C_V are given below.

$$U = 3/4pR\theta\{[2/(e^{\theta/T} - 1)] + [1/(e^{\theta/2T} - 1)]\}. \tag{10}$$

$$C_V = 3/4pR(\theta^2/T^2)\{[2e^{\theta/T}/(e^{\theta/T} - 1)^2] + [e^{\theta/2T}/2(e^{\theta/2T} - 1)^2]\}. \tag{11}$$

Table 3
List of input parameters used in the Grüneisen model for estimating the low-temperature thermal expansion of D9 stainless steel

Density at 300 K	7997 kg m^{-3}
Average molecular weight	56.405
Lattice parameter at 300 K	0.35903 nm
Debye temperature	456 K
Electronic specific heat coefficient	4.753×10^{-1} J kg^{-1} K^{-2}
Isothermal bulk modulus	158 GPa
Pressure derivative bulk modulus	2.81
Grüneisen parameter	1.2
Estimated C_P	487 J kg^{-1} K^{-1}
Q_0, the fit parameter in Eq. (6)–(8)	1.52×10^7 J kg^{-1}
p, the fit parameter in Eq. (10) and (11)	1.2

In the above equations, R represents the gas constant and the rest of the symbols assume their designated meaning. The constant p stands for the number of atoms per formula unit and for a pure metal takes the value of unity. But the present candidate material being both a substitutional and interstitial alloy, p must exceed one by a small value. A value of 1.2 is chosen so that the calculated C_V (assumed to be equal to C_P) is in agreement with the currently available experimental estimate [6].

At present no experimental estimate is available for B_0, B_0' and γ_G of our D9 stainless steel. As a rough approximation, we adopt a value of 158 GPa for B_0. This estimation follows from the knowledge of the correlation between room temperature bulk modulus (B_0) and density (ρ) of 316 and 304 steels [20]. The B_0' is estimated following Kouam and Rochegude [21]. Skipping the details, we may state that the Debye model proposed by Koum and Rochegude for volume thermal expansivity yields the following approximation connecting thermal expansivity (α_V), isobaric specific heat (C_P), molar volume (V_0), isothermal bulk modulus (B_0) and pressure derivative of bulk modulus (B_0').

$$\alpha_V = 1/3\{(B_0' + 1)C_P/(B_0 V_0)\}. \quad (12)$$

Eq. (12) is basically the same as the Grüneisen formula for α_V, if we assume that $\gamma_G = 1/3(B_0' + 1)$. By substituting for C_P, a value of 487 J kg^{-1} K^{-1}, obtained from the Debye model, we estimate B_0' to be 2.81. This in turn gives for γ_G a value of 1.17. It must be stated that the B_0' value estimated in the present study for D9 is well within the normal range of the reported values for similar austenitic stainless steels [22]. All the input data used in the calculation of low-temperature thermal expansion data are listed in Table 3.

The calculated low-temperature α_V is plotted in Fig. 3. As is clearly evident from this figure, the estimated low-temperature thermal expansion data merges reasonably smoothly with its high-temperature counterpart. In fact it must be admitted that the Grüneisen formalism has been used here as an empirical, yet physically plausible model. This is so, because the input parameters figuring in the model are treated as fitting parameters, although, the trial values to begin with were obtained from the existing data through standard approximations. A variation of about $\pm 10\%$ is considered for B_0' θ_D and γ_G. It is found that varying these adjustable parameters within the stated limits has not resulted in any appreciable quantitative change (the change in α_V is less than $\pm 5\%$) in the calculated thermal expansion data. On the other hand, the smoothness of the joining of the experimental high-temperature data with the simulated low-temperature one is sensitive to the choice of the parameter set. The set of input values quoted in Table 3 is therefore based on the criterion of ensuring a smooth thermal expansion curve from about 50–1300 K.

The estimated C_V using the Nernst–Lindemann expression in the temperature range 50–300 K is plotted in Fig. 4. It may be seen that the calculated C_V coincides more or less with the experimental values for 304 and 316 stainless steels. This is expected, since Debye temperatures of these stainless steels are rather close. One final point regarding the calculated α_V and C_V is that we have ignored the electronic contribution to these quantities. Although expected to be small, the electronic contributions are appreciable at low-temperatures. Further, any magnetic contribution possible due to the relatively high-nickel content of our steel is also not accounted for in our simulation. In this sense, our calculated low-temperature estimates represent lower bound values. In any case, considering the approximations inherent to the Grüneisen formalism, especially when it is treated with empirically adjusted inputs, the absolute values of our estimated low-temperature expansivity cannot be overemphasised. On the contrary, it may be considered as a physically meaningful first order approximation pending a full fledged experimental investigation.

Acknowledgements

The authors are grateful to Dr M. Vijayalakshmi, Dr V.S. Raghunathan, Dr P.R. Vasudeva Rao, and Dr Baldev Raj for their encouragement and keen interest in the present work. The authors thank Mr V. Shanmugam for providing us the D9-sample used in this study. Mr V. Srinivasan is thanked for getting us the compositional analysis of the sample through optical emission spectrometry. One of the authors, Dr R. Jose wishes to acknowledge the Department of Atomic Energy of India for awarding him the prestigious Dr K.S. Krishnan fellowship, as a part of which the present study is carried out.

References

[1] Selection of materials for PFBR nuclear steam supply system components, IGCAR Internal report PFBR/MDG/2002/001; See also S. Venkadesan, A.K. Bhaduri, P. Rodriguez, K.A. Padmanabhan, J. Nucl. Mater. 186 (1992) 117.

[2] L. Leibowitz, R.A. Blomquist, Int. J. Thermophys. 9 (1988) 873.

[3] S.L. Mannan, P.V. Sivaprasad, in: K.H.J. Buschow, R.W. Cahn, M.C. Flemings, B. Ilschner, E.J. Kramer, S. Mahajan (Eds.), Encyclopaedia of Materials Science and Engineering, vol. 3, Elsevier, New York, 2001, p. 2857.

[4] W. Kesternich, D. Meertens, Acta Metall. 34 (1986) 1071.

[5] L.K. Mansur, E.H. Lee, P.J. Maziasz, A.P. Rowcliffe, J. Nucl. Mater. 141 (1986) 633.

[6] H.P. Nawada, O.M. Sreedharan, V.S. Raghunathan, unpublished research, 2002.

[7] R.E. Taylor, in: C.Y. Ho (Ed.), Thermal Expansion of Solids, vol. I-4, ASM International, Materials Park, Ohio, 1998, p. 157.

[8] R.R. Reeber, K. Wang, Mater. Sci. Eng. R23 (1998) 101.

[9] B.D. Cullity, Elements of X-ray Diffraction, 2nd Ed., Addison Wesley, Reading, MA, 1978.

[10] P. Aldebert, J.-P. Traverse, High Temp.–High Press. 16 (1984) 127.

[11] J.C. Ho, G.B. King, F.R. Fickett, Cryogenics 18 (1978) 296.

[12] J.B. Wachtman, T.G. Scuderi, G.W. Gleek, J. Am. Ceram. Soc. 45 (1962) 310.

[13] I. Suzuki, J. Phys. Earth 23 (1975) 145.

[14] J.M. Corsan, N.I. Mitchem, Cryogenics 19 (1979) 11.

[15] NIST Cryogenic Materials Property Database *vide* Web Site. Available from <http://cryogenics.nist.gov/NewFiles/304L_SS.html>.

[16] A.P. Miiller, A. Cezairliyan, High Temp.–High Press. 23 (1991) 205.

[17] N.L. Perovic, K.D. Maglic, A.M. Stanimirovic, G.S. Vukovic, High Temp.–High Press. 27/28 (1995/1996) 53.

[18] J.H. Harding, D.G. Martin, P.E. Potter, EUR-12402 report, AERE, Harwell, UK, 1989, p. 85.

[19] A. Cezairliyan, A.P. Miiller, Int. J. Thermo. Phys. 1 (1980) 83.

[20] H.M. Ledbetter, J. Appl. Phys. 52 (1981) 1587.

[21] J. Kouam, P. Rochegude, J. Mater. Sci. Lett. 15 (1996) 600.

[22] D. Gerlich, S. Hart, J. Appl. Phys. 55 (1984) 880.